JOURNAL OF MATERIALS SCIENCE 32 (1997) 643–652

Characterization and sintering behaviour of submicrometre titanium dioxide spherical particles obtained by gas-phase hydrolysis of titanium tetrabutoxide

J. RUBIO, J. L. OTEO, M. VILLEGAS, P. DURAN
Instituto de Cerámica y Vidrio, 28500 Arganda del Rey, Madrid, Spain

Spherical fine (~ 0.7 μm) titania powders were prepared by vapour-phase hydrolysis of a titanium tetrabutoxide/butanol solution. Powder X-ray diffraction showed that as-prepared powders were amorphous and crystallized to anatase when calcined at 450 °C. Although the spherical titania particles shrank on calcination and retained the spherical shape, the primary particles grew to a notable extent after calcining. The individual calcined titania spheres were constituted by microporous agglomerates of about 13 nm primary anatase particles. When isopressed at 200 MPa, the titania spheres were crushed to form dense green bodies ($\sim 55\%$ theoretical density). These green compacts gave dense bodies ($> 99\%$) of rutile when sintered at 1030 °C for 2 h with a submicrometre and quite uniform microstructure.

1. Introduction

Over the last decade, much research worldwide has focused on learning to control the arrangement of matter at ever-smaller dimensions. This technology involves the use of materials having properties much better than those of conventional metals and ceramics. Monodispersed spherical ceramic particles, having a very high sinterability, can be used as starting raw materials for making advanced ceramics with controlled and submicrometre microstructures and, therefore, with improved performances. However, the microstructure developed during the sintering of such improved ceramics is strongly determined by the powder characteristics such as particle size, size distribution, agglomeration state and, finally, the green body microstructure.

From the first studies of Sacks and Tseng [1, 2] on the sintering of monodispersed silica particles prepared by the alkoxide hydrolysis method, many kinds of monodispersed particles of only one component have been synthesized [3–8]. Because of the different hydration rate of each metal alkoxide, the synthesis of monodispersed powders containing two or more metal elements becomes much more difficult. In spite of this Y-TZP [9], YSZ [10], mullite [11] and PZT [12] monodispersed spherical powders have been prepared by the controlled hydrolysis of alkoxides. Matijevic and co-workers [13, 14] have established the colloidal chemistry leading to the obtaining of monodispersed single oxide powders, and the best conditions, with some limitations, for achieving uniform-sized monodispersed powders were established by Barringer and Bowen [15]. The production of well-dispersed small particles (< 1 μm) with a narrow size distribution is, therefore, probably the more suitable way to achieve an ideally sinterable powder leading to ceramics theoretically dense at low temperature with a uniform and fine-grained microstructure. This being so, it is also true that amorphous nanometre-sized ceramic particles, when calcined, presents some problems in forming dense green ceramic bodies with good packing uniformity [16, 17]. On the other hand, subsequent to publication of Ruthner's paper [18] establishing the industrial applicability of the spray-roasting technique to the synthesis of MgO and ferrites, many papers [19–22] have been devoted to obtaining spherical fine ceramic powders by using the spray-pyrolysis synthesis technique, in spite of several impediments to achieve both a narrow particle-size distribution and a controlled particle morphology. The purposes of the present work were to present the preliminary results of a simple preparation method of spherical TiO_2 particles by hydrolysis in the vapour-phase of relatively highly concentrated titanium tetrabutoxide solutions, powder characterization, compaction behaviour, and the sintering behaviour of the obtained green compacts.

2. Experimental procedure

Fig. 1 schematically shows the experimental apparatus used to prepare the spherical TiO_2 particles. The titanium alkoxide $[Ti(C_4H_9O)_4 \cdot C_4H_9OH]$ was placed in a glass container thermostatically controlled at 180 °C, and deionized water was placed in another one, thermostatically controlled at 75 °C. Both were slightly pressurized with nitrogen gas to spray through a glass nozzle with several openings of

0022–2461

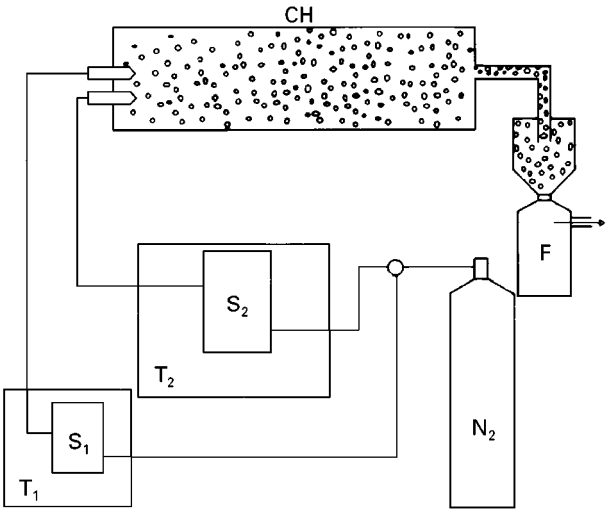

Figure 1 Schematic drawing of the apparatus for phase-vapour hydrolysis. T_1, Thermostat 1; T_2, thermostat 2; S_1, nebulizer 1; S_2, nebulizer 2; CH, hydrolysis chamber; F, filter.

400 μm diameter into a hydrolysis chamber. The temperature of the hydrolysis chamber was about 25 °C, and the sprayed jets of both the titanium tetrabutoxide and the deionized water rapidly reacted as they came into contact to form spherical TiO_2 particles. In order to ensure a complete reaction, a water/titanium butoxide molar ratio $\geqslant 3$ was maintained during the hydrolysis process. The powders were collected from the hydrolysis chamber by filtering through a filter paper. Then the powder was washed with isopropyl alcohol, filtered and dried at 120 °C. The dried powder was slowly calcined at 450 °C for 2 h, isopressed at 100 MPa (compacts A), or at 200 MPa (compacts B). After isopressing the two kinds of green compacts were sintered in air in the temperature range 600–1400 °C for 2 h.

Particle size, particle-size distribution and shape of the particles were studied by scanning electron microscopy (Carl Zeiss DSM-950). Specific surface area was determined by the BET method with nitrogen as adsorbate gas (Accusorb 210E, Micromeritics). The thermal behaviour of the as-prepared powders was investigated by differential thermogravimetric analysis (DTA-TG, Netzsch STA-409) in air at a heating rate of 8 °C min^{-1}. The crystalline phases for TiO_2 were studied by X-ray diffraction (Siemens D5000) with CuK_α radiation. The crystallite size of calcined powders was calculated from the Scherrer equation by means of the X-ray line broadening method [23]. The average particle size was determined on 300 particles randomly extracted from the scanning electron micrographs.

Fourier transform–infrared spectroscopy (FT–IR) was used to determine the presence of the wash solvent on the ground powders. An FT–IR spectrometer (Perkin–Elmer 1760X model), with a dry air purge, was used. Powder samples were mixed with dry KBr and the FT–IR cell purged for 20 min prior to spectral collection. A precision better than 4 cm^{-1} was obtained in all the measurements.

The pore-size distribution in the green compacts was studied by means of a porosimeter (Autopore II 9215 Micromeritics). Sintering kinetics were determined by constant heating rate (CHR) dilatometry by using a dilatometer (Netzsch DIL 402E/7) at a heating rate of 5 °C min^{-1} from 200–1400 °C.

Densities of the TiO_2 sintered bodies were measured by the Archimedes' method with water as the submersion liquid. The relative density was based on the theoretical density of 4.26 g cm^{-3}. The microstructure and the grain-size measurements were performed on the thermally etched polished surface samples by means of the SEM.

3. Results and discussion

3.1. Powder characterization

Fig. 2 shows XRD patterns of as-prepared and calcined powders. The XRD pattern of as-prepared powder was amorphous, and after calcining at 450 °C for 2 h showed only the broad XRD pattern of TiO_2 anatase phase. The XRD pattern of powders calcined above 800 °C showed the sharp peaks of TiO_2 rutile phase.

Fig. 3 shows TG–DTA curves of synthesized titania powders in air up to 1200 °C. The as-prepared

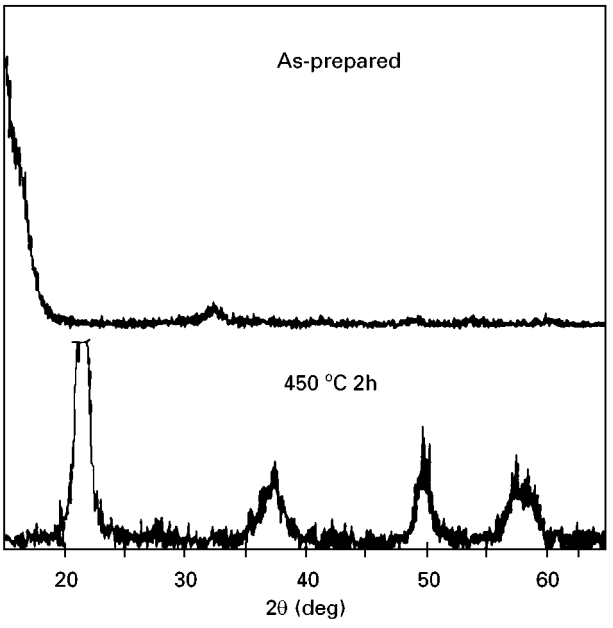

Figure 2 XRD patterns of as-prepared powders and powders calcined at the temperatures indicated.

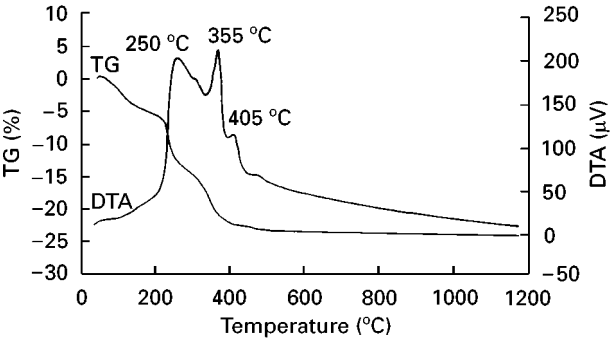

Figure 3 DTA–TG curves of monodispersed titania precursor powders.

powders have ~23% weight loss. The weight loss up to around 180 °C is due to the dehydration of the hydrous TiO_2 particles. The weight loss between 200 and 500 °C is due to the decomposition of residual organic species such as butoxy groups (OC_4H_9) and butanol. The main weight loss in the TG curve coincides with the two exothermic peaks in the DTA curve at 250 and 355 °C, due to the combustion of the organic groups remaining inside the TiO_2 particles. A third exothermic peak was present at 405 °C in the DTA curve, which is probably related to the condensation of Ti–OH groups with the subsequent release of water and the phase transformation from amorphous to anatase.

Infrared absorption spectra of the TiO_2 precursors dried at 120 °C and calcined at 1200 °C are given in Fig. 4. The precursors which had been dried at 120 °C show several peaks. The peaks around 3410 and 1640 cm^{-1} are due to the OH stretching and bending, respectively. The two peaks at about 2920 cm^{-1} are related to the stretching frequency for CH bonds. The weaker peaks between 1440 and 1355 cm^{-1} are associated with the bending of C–H bonds. This spectrum indicates that in the precursor powder there is a significant amount of organic material apparently from butyl alcohol or from butoxy groups which remain in the interior of the TiO_2 spherical particles. Heat treatment at high temperature (1200 °C) causes elimination of peaks due to OH, CH, C–OH and C–O–Ti, and the subsequent development of Ti–O–Ti absorption peaks at 470 and 645 cm^{-1} typical of TiO_2 phase.

From the above results, we can conclude that the precursor powders mainly formed a complex compound between titanium and the organic constituents and not a simple titanium hydroxide. From the DTA and infrared experiments, it seems that the organic constituents retain their basic chemical structure in the precursor phase. Such organic materials decompose on heating leading to the TiO_2 anatase phase or the TiO_2 rutile phase above 800 °C.

The particle shape of the precursor powders was observed by a scanning electron microscope and, as shown in Fig. 5, the powder was composed of nearly single-dispersed spherical particles having a relatively narrow size distribution, see Fig. 6, with an average particle size of approximately 700 nm. The surface of the as-prepared single-dispersed titanium dioxide particles was smooth. However, the surface of the spheres dried at 120 °C for 2 h was rough and many near nanometre-sized (~150 nm) particles or agglomerates were formed, see Fig. 7. After calcining, the SEM measured particle size was much larger than the crystallite size determined by the XRD line broadening method (12.5 nm), but the latter is in good agreement with the average particle size calculated from the BET surface area (13.5 nm). This crystallite size value was calculated taking into account the equation

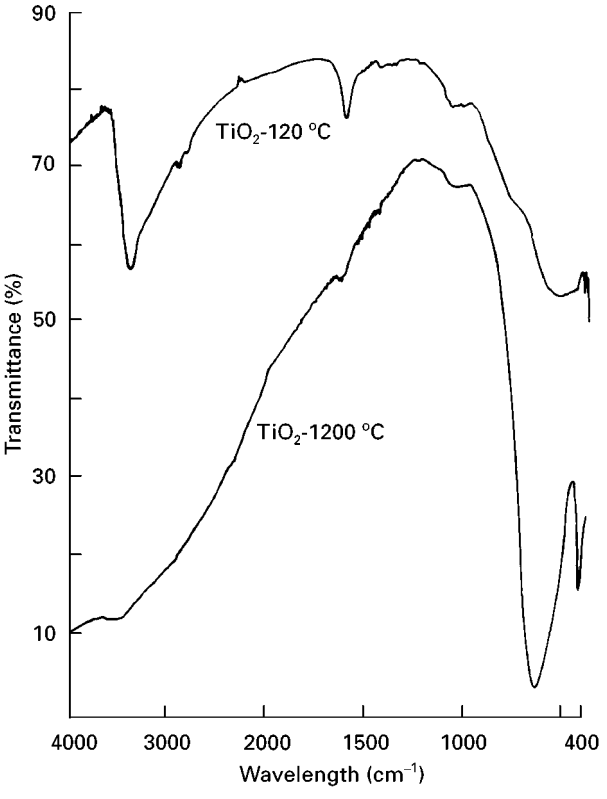

Figure 4 FT–IR spectra of dried monodispersed titania powders and powders calcined at the temperatures indicated.

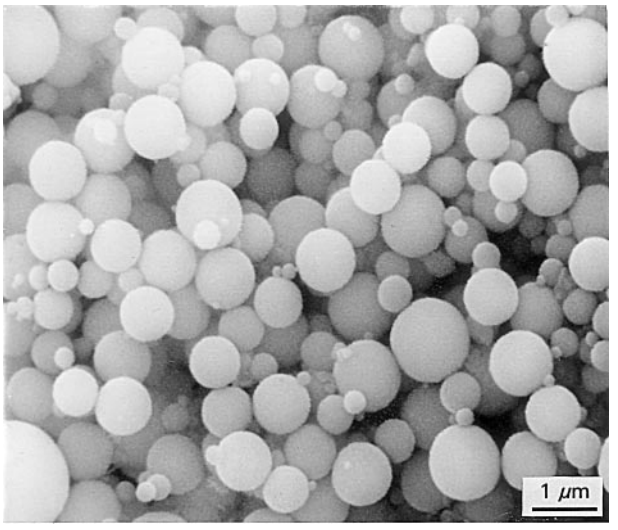

Figure 5 Scanning electron micrograph of monodispersed titania precursor powders.

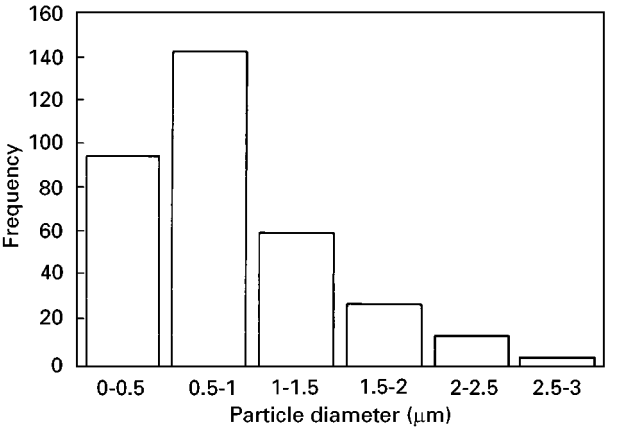

Figure 6 Particle-size distribution of monodispersed titania precursor powders.

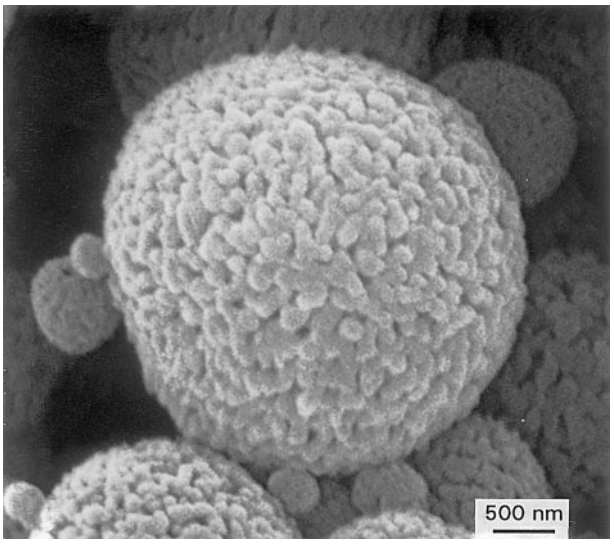

Figure 7 Microstructure of the dried monodispersed titania particles.

TABLE I Physical properties of the spherical TiO_2 powders

	Amorphous	Calcined
Average particle size (nm) (SEM)	700	450
Specific surface area (m^2g^{-1}) (BET)	180	114
Average particle size (nm) (from BET)	7.5	13.5
Crystallite size (nm) (XRD l.b.)	–	12.5

$D = 6/(\rho_t S_{BET})$ in which ρ_t is the theoretical density. It must also be mentioned that in the BET determination with nitrogen as adsorbate gas, the adsorption/desorption curves showed evidence for spherical TiO_2 particles with a microporosity in which the pore radius was less than 1 nm. This fact means that during the calcining process, microporosity was moving out from the interior of the small particle agglomerates to the boundary, with simultaneous small shrinkage. Given that the measured particle size by the XRD line broadening on the calcined powders was much smaller than that measured by SEM, it can be concluded that the observed particles in the surface of the spherical TiO_2 particles were agglomerates of the smaller TiO_2 ones. Table I shows the physical characteristics of the amorphous powder and that calcined at 450 °C.

3.2. Thermal evolution morphology of the spherical TiO_2 particles

The microstructural changes of the titanium-containing spheres were examined by SEM after successive thermal treatments. After washing with isopropyl alcohol and drying at 50 °C, the average particle size was about 0.7 μm and their surface was smooth, see Fig. 5. After drying in air at 120 °C for 2 h, the morphology of the spheres changed dramatically, as shown in Fig. 8a, from uniform and amorphous to granular, porous and rough, as a consequence of the partial dehydration produced at this temperature. After calcining at 450 °C, the diameters of the spheres were reduced, see Fig. 8b, and some overlapping areas

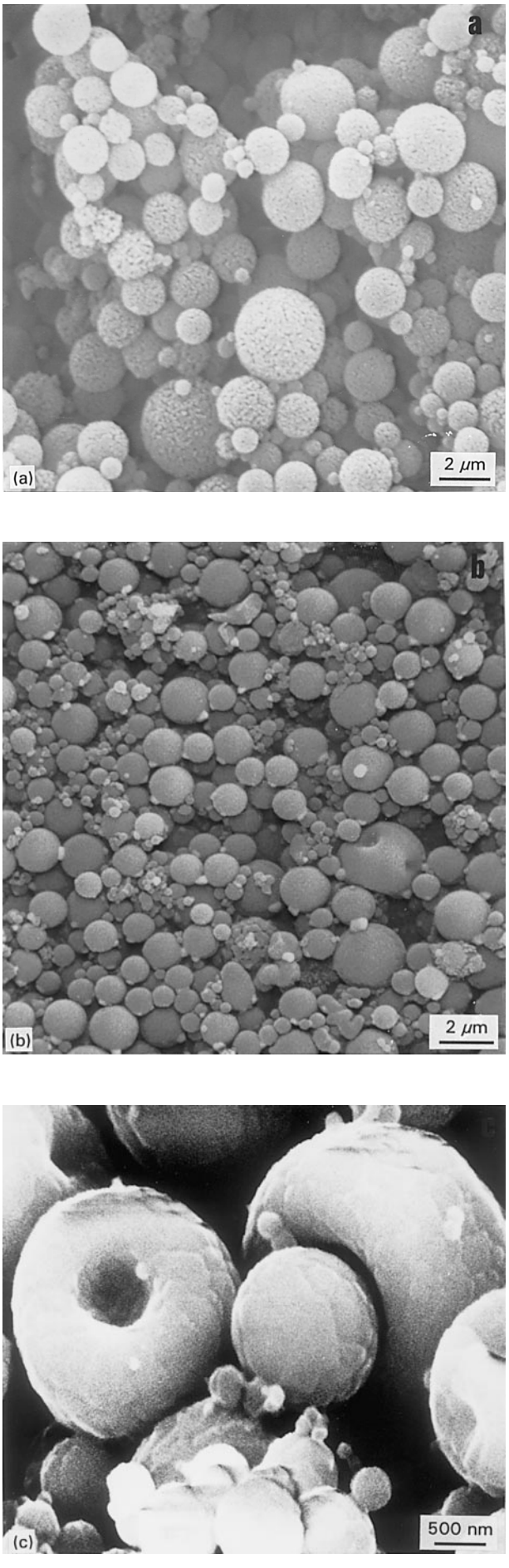

Figure 8 Morphology evolution of the monodispersed titania particles heat treated at (a) 120 °C, (b) 450 °C and (c) 1000 °C.

between them appeared. At high temperature ($\sim$1000 °C) the TiO_2 particles still retained the spherical shape but some shrinkage and cracking took place. The primary particles grew and sintered with each other to some extent, see Fig. 8c.

The size distribution of these spherical TiO_2 particles was wider than those prepared by the "controlled hydrolysis method" [3, 10]. Fig. 9 shows the evolution of the particle size with temperature treatment. The distributions were obtained from the SEM image. The size distribution was relatively narrow with an average particle size of about 0.4 μm after drying at 120° C. After calcining at 450 °C, the particle size decreased, many of the particles with the higher sizes disappeared and the number of fine particles increased. Such an apparently anomalous phenomenon could be justified by two factors; the shrinkage due to the release of water from the condensed Ti–OH groups or the associated water molecules, and the shrinkage related to the amorphous particles (density $= 2.56\,g\,cm^{-3}$) to anatase (density $= 3.89\,g\,cm^{-3}$) transformation. When the spheres were calcined at 1000 °C, the size of each sphere slightly increased, and some of them possessed many small grains and a porous or hollow core. The average size of these grains was $\sim$0.2 μm with a relatively regular polyhedra shape. This feature means that the poorly controlled evaporation of the organic species at low temperature could lead to the nucleation of small TiO_2 crystallites in the surface of the spheres during heating. These TiO_2 crystallites could give rise to the formation of a relatively hard spherical shell which prevented the collapse of spheres into compact solids at low temperature. Further heating at relatively higher temperatures would lead to the grain growth in the spheres, the core region became less dense and, finally, resulted in the formation of a hollow or porous sphere.

3.3. Compaction and sintering behaviour

The relative density of the spherical TiO_2 powder samples isopressed at 100 MPa (compacts A), was 48%, and that of the isopressed at 200 MPa (compacts B), $\sim$55%. Fig. 10a and b shows the fracture surfaces of both green compacts in which the spherical shape of as-prepared powder was partially kept after isopressing in the first case and completely crushed in the second one. Fig. 11 shows the pore-size distribution in both kinds of green compacts. In the low isopressed compacts, the curve had two peaks. The first one located at $\sim$30 nm is due to the pores formed between spheres, and the second one at 6 nm is the pores formed between the primary particles. In the high isopressed compacts, a homogeneous pore-size distribution curve with the main pore size about 18 nm, was found. It is evident from the curves that in the higher isopressed compacts, a shrinkage of the larger pores took place.

Fig. 12a and b show the non-isothermal sintering behaviour of the two kinds of green compacts. In the first one the shrinkage rate curve showed two maxima, one at 925 °C, which is related to the elimination of the smaller pores, and the other at about 1230 °C,

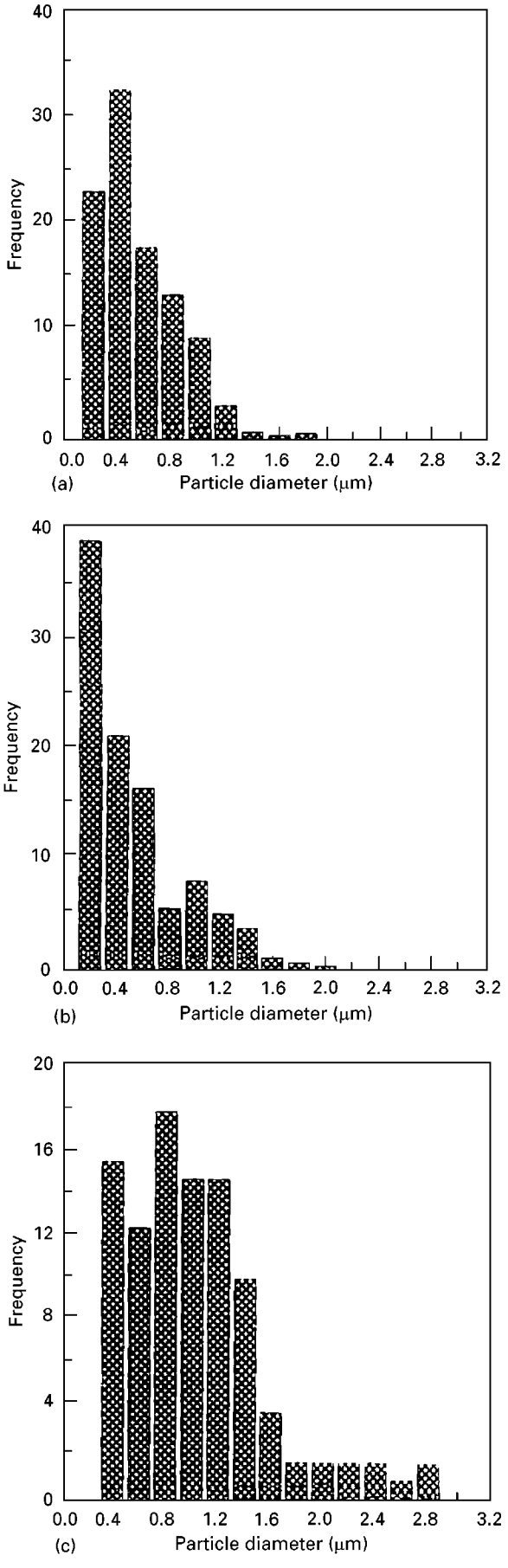

Figure 9 Particle-size distribution of titania powders heat treated at (a) 120 °C, (b) 450 °C, and (c) 1000 °C.

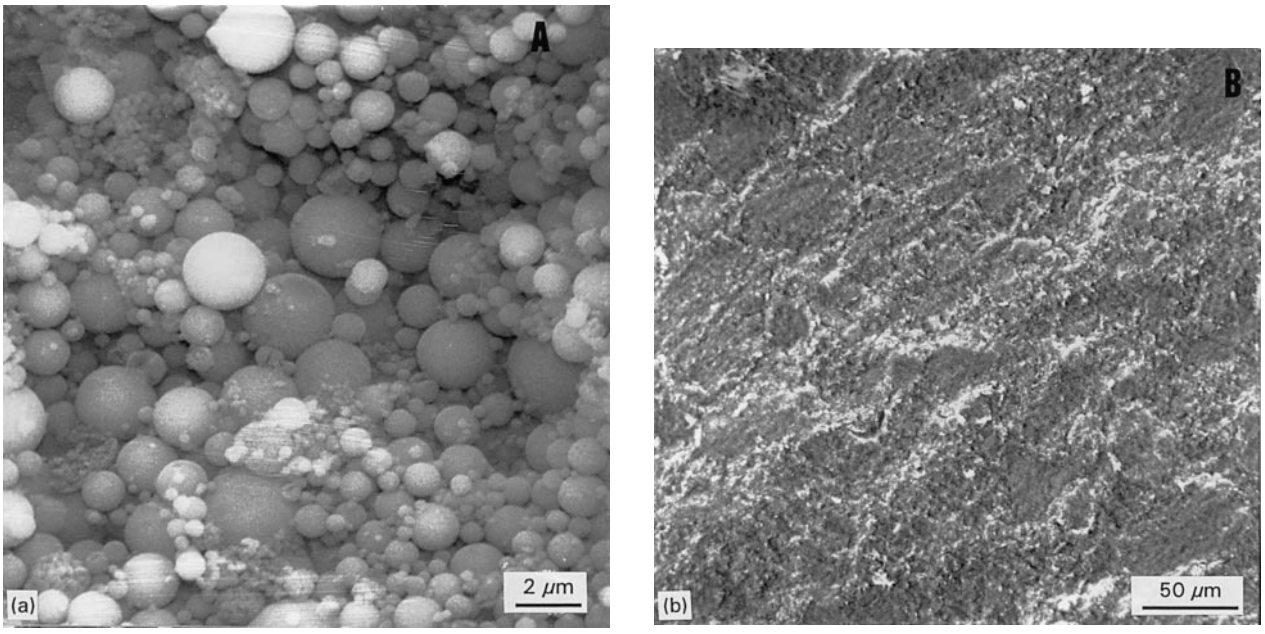

Figure 10 Fracture surfaces of green compacts A and B isopressed at (a) 100 MPa, and (b) 200 MPa, respectively.

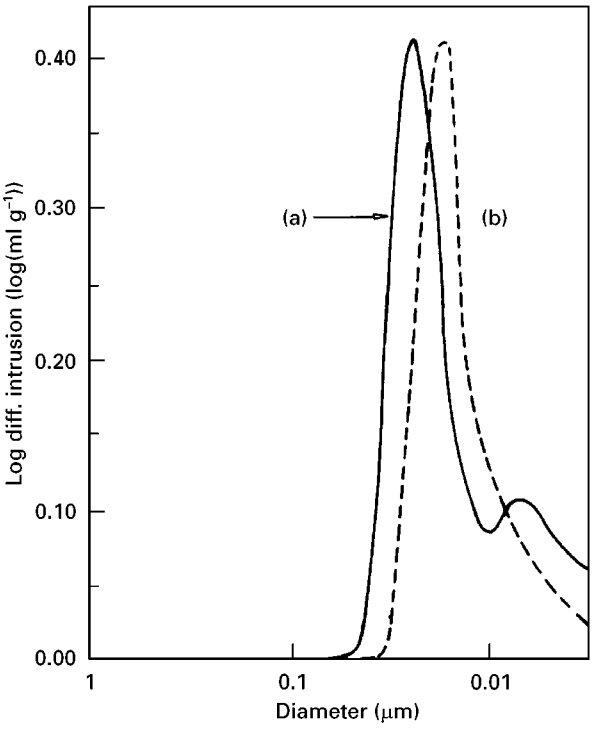

Figure 11 Pore-size distribution curves of the two kinds of green compacts (a) 100 MPa, and (b) 200 MPa.

corresponding to the maximum of the densification rate. In the case of the highly isopressed compacts, curve b in Fig. 12, only one maximum in the shrinkage rate curve was found. The location of such a maximum was at a temperature, $\sim 1030\,^{\circ}C$, much lower than that of the low isopressed compacts, proving the high sinterability of the prepared compacts. The enhanced sinterability of these compacts could be related to the small size of the primary particles and their uniform packing in the green bodies.

Fig. 13 shows the density variation with sintering temperature of green compacts A and B. The sinterability of compacts B is much higher than that of the compacts A and this fact could be closely related to the smaller particle size and narrower pore-size distribution. The relative density reached $\sim 96\%$ theoretical at a temperature as low as $830\,^{\circ}C$ which is $300\,^{\circ}C$ lower than that necessary to attain the same relative density in compacts A, and $400\,^{\circ}C$ lower than the normal sintering temperature used for commercial TiO_2 powders [24]. At $\sim 1030\,^{\circ}C$ the relative density of compacts B was $\sim 99\%$ theoretical and this became constant for higher temperatures. These density values are somewhat lower than those reported elsewhere [10–24], and it could be related to both the relatively higher particle size of the present TiO_2 powders and the wider pore-size distribution in the green compacts.

Given that the maximum densification rate was attained at 1230 and $1030\,^{\circ}C$ for compacts A and B, respectively, the isothermal sintering experiments were carried out at those temperatures. Fig. 14 shows the density change and, as can be seen, sintered bodies of compacts B reached $> 99\%$ theoretical density within the first 5 min. No more then 96% dense bodies were achieved in compacts A in the same sintering time.

Fig. 15 shows the microstructural evolution of compacts A as a function of the sintering temperature. In compacts sintered at $1000\,^{\circ}C$ (a), many interagglomerate sintering areas can be observed with no exaggerated grain growth if compared with the original particle size. At $1200\,^{\circ}C$ (b), a strong decrease in porosity is present and the measured grain size was about 3 μm. In Fig. 15c the fracture surface of the same sample can be seen. All the pores are located at the grain boundaries and the triple-grain points. The fracture is of transgranular mode.

Fig. 16 shows the polished and fracture surfaces for compacts B sintered at 800 and $1030\,^{\circ}C$ for 2 h. The microstructure in (a) is quite uniform. The particle size is less than 1 μm with some significantly larger

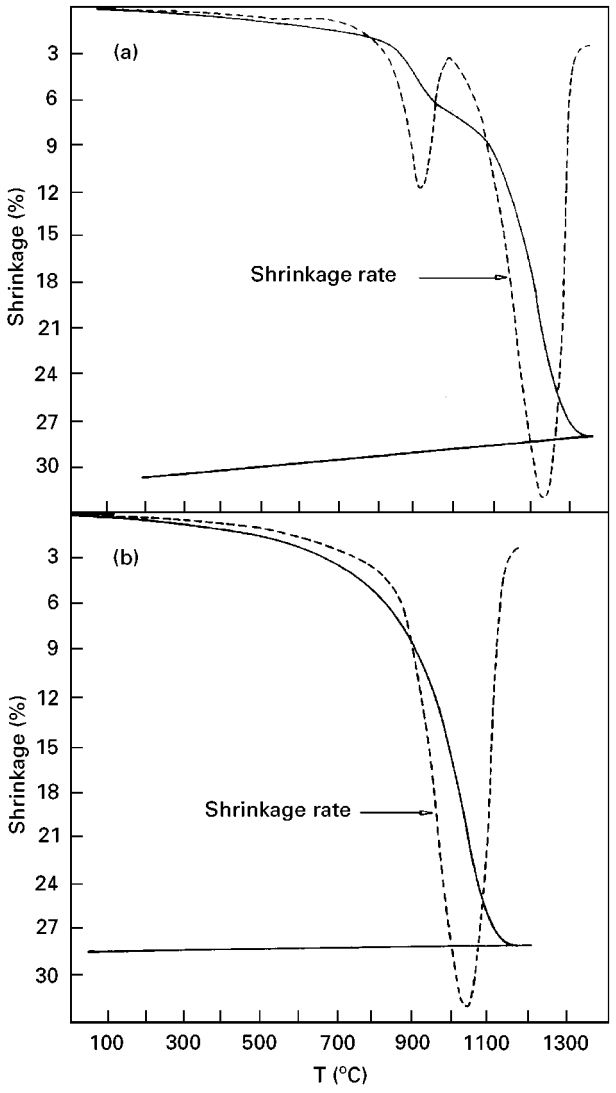

Figure 12 Shrinkage behaviour of green compacts. (a) A and (b) B.

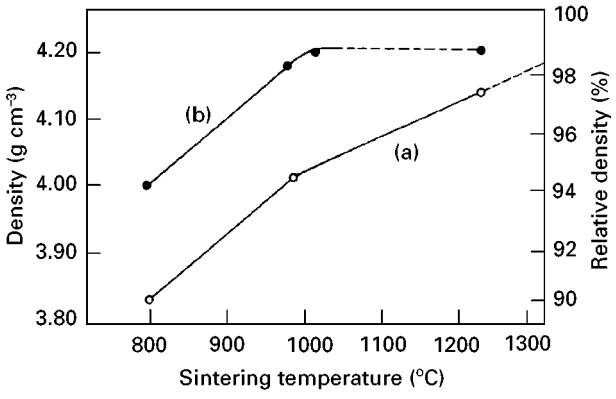

Figure 13 Density variation of (a) 100 MPa and (b) 200 MPa compacts A and B, respectively, with sintering temperature for 2 h.

particles. In Fig. 16b, an evident change in morphology of the particles took place, and elongated and faceted particles can be observed. The particle size grew to about 2 μm in the smaller dimension (the length was twice this value), and the distribution of the particle size was much wider than that at 800 °C. The fracture surface of the compact sintered at 1300 °C is shown in

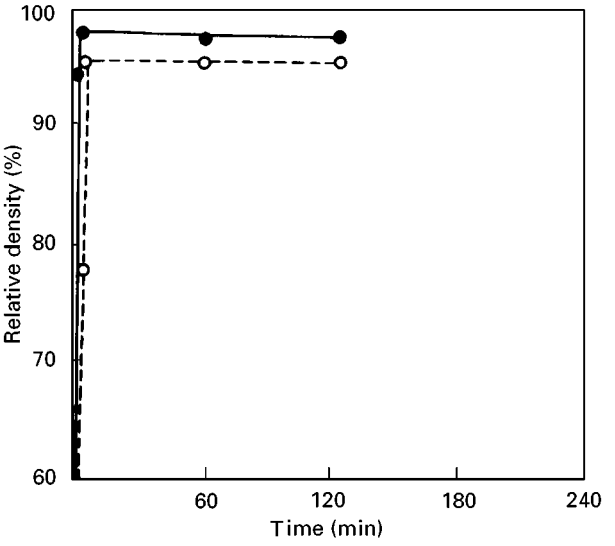

Figure 14 Isothermal sintering of (○) compacts A at 1230 °C and (●) compacts B at 1030 °C.

Fig. 16c. This shows the transgranular mode and some pores seemed to be at the interior of the grains.

4. Discussion

The preparation of spherical TiO_2 particles with a relatively narrow size distribution has been carried out by hydrolysis in the vapour phase of titanium tetrabutoxide with a relatively high alkoxide concentration. The crystallization and microstructural changes of spherical, ~0.7 μm in size, titania particles upon heating have been studied. The results indicated that the monodispersed titanium dioxide particles were amorphous and constituted by many small (near nanometre-size) particles of anatase which crystallized on calcining at 450 °C.

Although some spherical titania particles deformed during the heat treatment, indicating that they could be hollow, the majority of them were solid in spite of the relatively high alkoxide concentration. This fact indicates both the adequate viscosity and polymerization degree of the alkoxide [20]. A better control of the initial relative saturation will lead to smaller spherical particles being obtained with a narrower size distribution [25].

Observation of the individual titania spheres indicates that these retained the spherical shape after calcining at 450 °C as consequence of a slow sequential dehydration and elimination of organic species during the calcination process. Simultaneously, many nuclei were formed leading to the formation of small packed agglomerates (secondary particles) constituted by primary anatase nanometre-size (~13 nm) particles [26, 27]. Heating to higher temperatures induced grain growth, resulting in a solid polycrystalline spherical particle (Fig. 17).

In view of the agglomerates which form the spherical anatase particles, and assuming that both the agglomerates are soft and the attractive forces between primary particles are weak [29], a rupture of the initial spherical particle, to give non-agglomerated

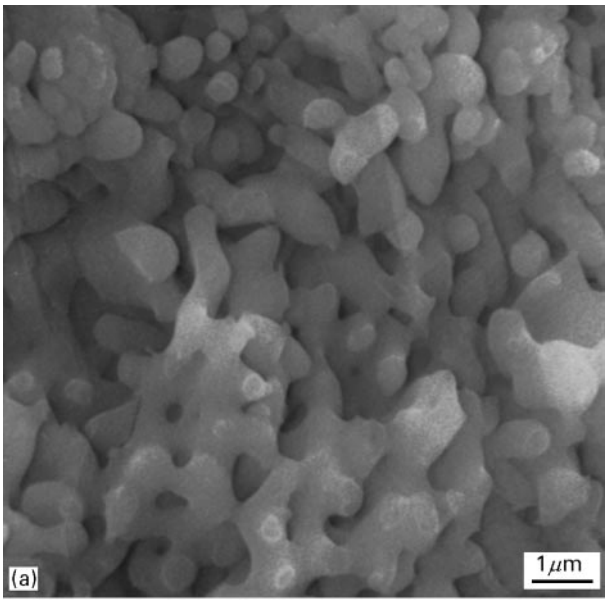

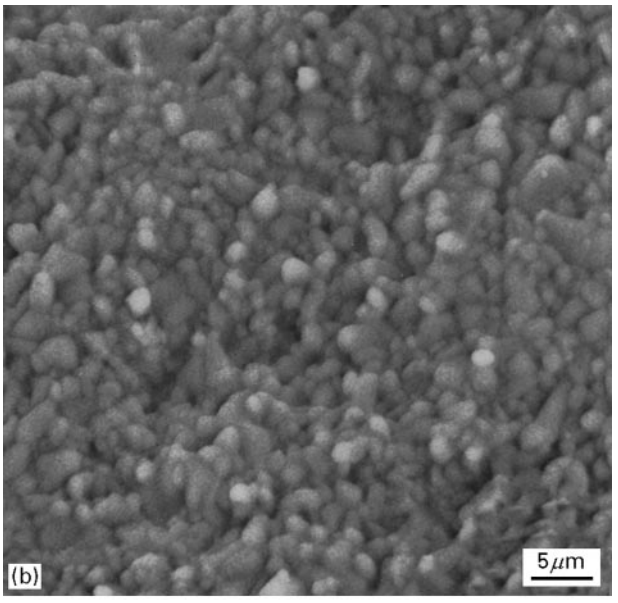

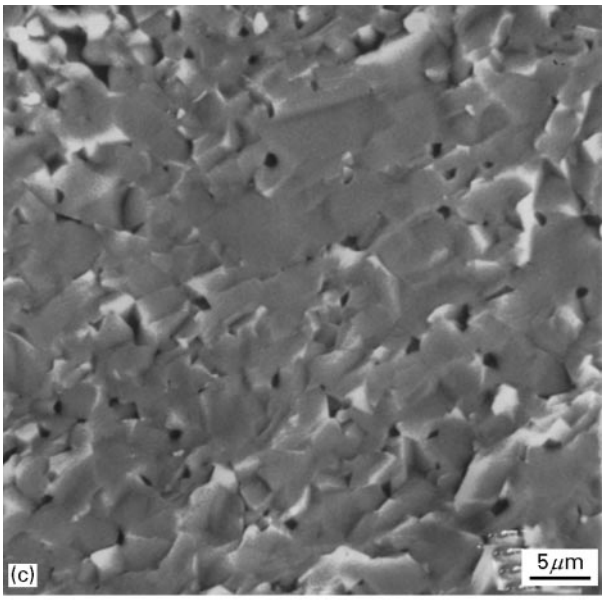

Figure 15 Microstructural evolution of compacts A sintered 2 h at (a) 1000 °C, (b) 1200 °C and (c) 1200 °C fracture surface.

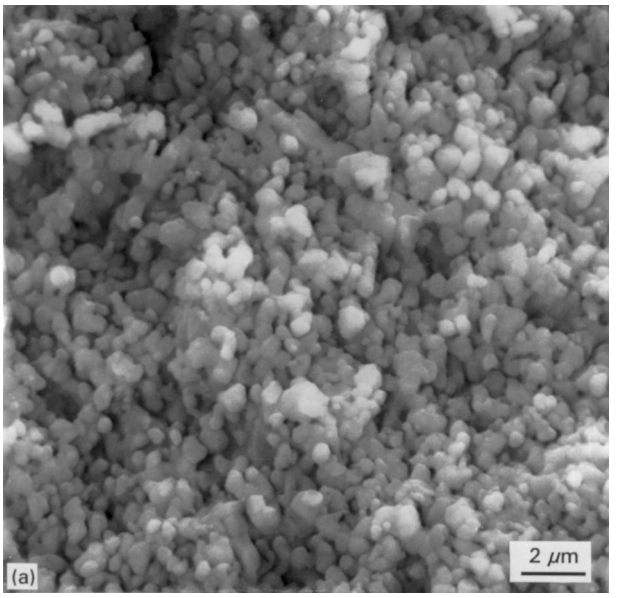

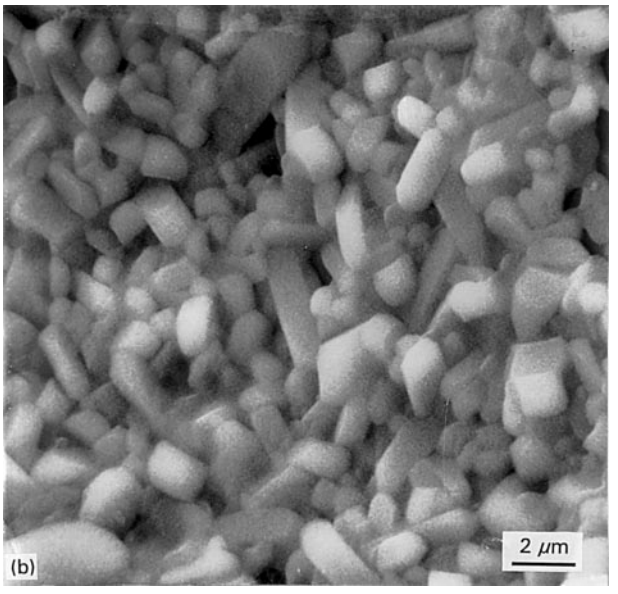

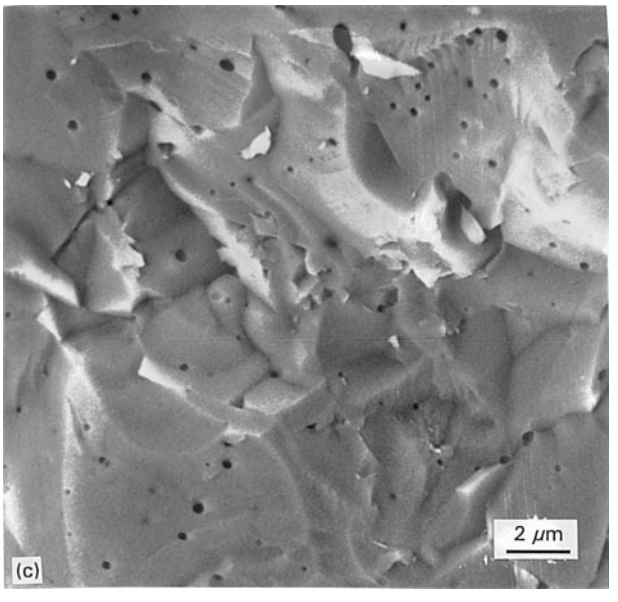

Figure 16 Microstructural evolution of compacts B sintered 2 h at (a) 800 °C, (b) 1030 °C and (c) 1300 °C fracture surface.

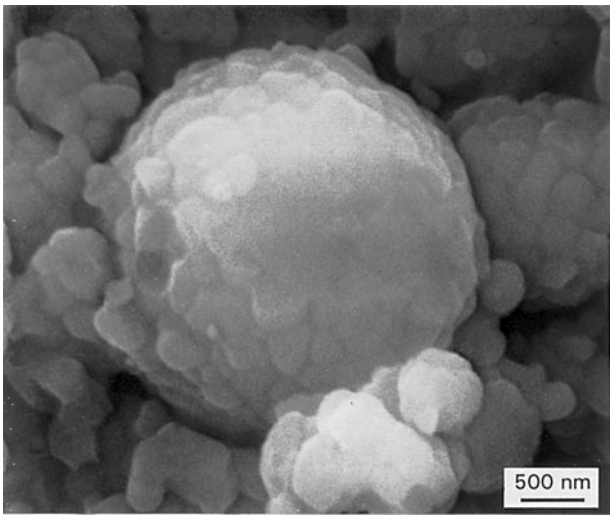

Figure 17 Solid spherical titania particles after sintering at 1000 °C.

nanoparticles by isostatic compaction, would be possible. In fact, the observation of the green compacts fracture surface showed evidence, see Fig. 10, for partial or completely crushed spherical particles at 100 and 200 MPa, respectively, thus confirming the above assumption. The degree of mutual accommodation of the nano-particles would give rise to green compacts having both a high green density and a narrow pore-size distribution. The high densification level (55% theoretical) reached in the 200 MPa green compacts, although is very different from the value for packing of spherical submicrometre particles ($\sim$64%) [30, 31], is in good agreement with the data of Oguri *et al.* [32] for packing of nanometre-sized anatase particles by filter-casting.

Compaction of calcined spherical titania particles eliminates the large volume change accompanying crystallization and, thus, the total shrinkage of the green compacts after sintering was never higher than 30%, see Fig. 12a and b. As it was shown the 200 MPa compacts sintered at a temperature $\sim$300 °C lower than the 100 MPa green compacts. The higher sinterability of those green compacts, having the same primary particle size, can be attributed to the smaller pore size and narrower pore-size distribution. Thus a significant densification takes place at about 650 °C in compacts B, while this phenomenon was not present up to $\sim$ 800°C in compacts A. In spite of this, a rapid densification took place in the short temperature range of 180 °C, between 830 and 1030 °C and between 1050 and 1230 °C, for the two kinds of green compacts, although the final density was very different in both cases. A pore-coarsening phenomenon, which retarded the densification process of the compacts A, led to less dense bodies. It is believed that the enhanced densification in the case of compacts B, with a parallel slow grain-growth process, took place by a grain-boundary diffusion mechanism as reported by Anderson [33] and Barringer *et al.* [34].

As shown above, see Fig. 15, no rapid grain growth took place at or below 96% dense compacts and an exaggerated grain-growth process, not shown here, occurred for higher densities. Although the grain size was relatively small ($\leqslant 1$ μm) the particle-size distribution and green-bodies packing were rather wide and relatively uniform, and these two factors could be the reason for the exaggerated grain growth observed at higher densities [17, 32]. According to our results, it seems to be that the larger grains grew at the expense of the smaller ones [35], as a consequence of the presence of multiparticle arrays within the ceramic matrix.

5. Conclusion

Spherical amorphous titania particles have been prepared by vapour-phase hydrolysis of a titanium-tetrabutoxide $Ti(OC_4H_9)_4 \cdot OHC_4H_9$ solution, and their main sizes were in the range 0.1–1.4 μm. The individual titania spheres were constituted by microporous agglomerates of about 13 nm primary particles which transformed to crystalline anatase at approximately 405 °C. On calcining at 450 °C, the spherical titania particles retained their shape and, after isopressing, the spheres were crushed to many anatase nanometre-sized particles leading to green compacts with a density and pore-size distribution depending on the pressing pressure. The denser green compacts (200 MPa) led to almost fully dense bodies (>99% theoretical density) at a temperature as low as 1030 °C for 2 h, with a submicrometre and quite uniform microstructure.

References

1. M. D. SACKS and T.Y. TSENG, *J. Am. Ceram. Soc.* **67** (1984) 526.
2. *Idem*, *ibid.* **67** (1984) 532.
3. B. FEGLEY and E. A. BARRINGER, in "Better Ceramics through Chemistry", Vol. 32, edited by C. T. Brinker, (Materials Research Society Symposia Proceedings, Elsevier, NY, 1984) p. 187.
4. E. A. BARRINGER and H. K. BOWEN, *Langmuir* **1** (1985) 414.
5. T. OGIHARA, N. MIZUTANI and M. KATO, *Ceram. Int.* **13** (1987) 35.
6. M. LI and G. L. MESSING, in "Ceramic Powder Science III", edited by G. L. Messing, S. I. Hirano and H. Hausner (American Ceramic Society, Westerville, OH, 1990) p. 129.
7. T. OGIHARA, H. NAKAJIMA, T. YANAGAWA, N. OGATA, K. YOSHIDA and M. MATSUSHITA, *J. Am. Ceram. Soc.* **74** (1991) 2263.
8. Y. T. MOON, H. K. PARK, D. K. KIM and C. H. KIM, *ibid.* **78** (1995) 2690.
9. H. ISHIZAWA, O. SAKURAI, N. MIZUTANI and M. KATO, *Am. Ceram. Soc. Bull.* **65** (1986) 1399.
10. B. FEGLEY, P. WHITE and H. K. BOWEN, *ibid.* **64** (1985) 1115.
11. T. OGIHARA, T. YANAGAWA, N. OGATA, K. YOSHIDA, M. IGUCHI, N. NAGATA and K. OGAWA, *J. Ceram. Soc. Jpn* **102** (1994) 778.
12. H. B. KIM, J. H. LEE and S. J. PARK, *J. Mater. Sci. Mater. Electron.* **6** (1995) 84.
13. E. MATIJEVIC, M. BUDNICK and L. MEITES, *J. Coll. Interface Sci.* **61** (1977) 302.
14. R. BRACE and E. MATIJEVIC, *J. Inorg. Nucl. Chem.* **35** (1973) 3691.
15. E. A. BARRINGER and H. K. BOWEN, *J. Am. Ceram. Soc.* **67** (1982) c-199.
16. L. H. EDELSON and A. M. GLAESER, *ibid.* **71** (1988) c-198.
17. *Idem*, *ibid.* **71** (1988) 225.

18. M. J. RUTHNER, in "Ceramic Powders", edited by P. Vincenzini (Elsevier, Amsterdam, The Netherlands, 1983) p. 515.
19. D. M. ROY, R. R. NEURGAONKAR, T. P. HOLLERAN and R. ROY, *Am. Ceram. Soc. Bull.* **56** (1977) 1023.
20. S. C. ZHANG, G. L. MESSING and M. BORDEN, *J. Am. Ceram. Soc.* **73** (1990) 61.
21. D. W. SPROSON, G. L. MESSING and T. J. GARDNER, *Ceram. Int.* **12** (1986) 3.
22. T. Q. LIU, O. SAKURAI, N. MIZUTANI and M. KATO, *J. Mater. Sci.* **21** (1986) 3698.
23. K. P. KLUG and L. E. ALEXANDER, "X-Ray Diffraction Procedures", (Wiley, New York, 1974).
24. M. F. YAN, *Mater. Sci. Eng.* **48** (1981) 53.
25. G. L. MESSING, S. C. ZHANG and G. V. JAYANTHI, *J. Am. Ceram. Soc.* **76** (1993) 2707.
26. G. L. MESSING and S. C. ZHANG, in "Euro-Ceramics II", edited by G. Ziegler and H. Hausner (Deutsche Keramische Gesellschaft, Cologne, Germany 1993) p. 185.
27. M. KONDO, K. SHINOKAZI, R. OOKI and N. MIZUTANI, *J. Ceram. Soc. Jpn* **102** (1994) 742.
28. T. IKEMOTO, K. UEMATSU, N. MIZUTANI and M. KATO, *Yogio Kyokaishi* **93** (1985) 261.
29. M. KONDO, H. FUNAKUBO, K. SHINOZAKI and N. MIZUTANI, *J. Ceram. Soc. Jpn* **103** (1995) 552.
30. J. D. BERNAL and J. MASON, *Nature* **188** (1960) 908.
31. P. N. PUSEY and W. VAN MEGEN, *ibid.* **320** (1986) 340.
32. Y. OGURI, R. E. RIMAN and H. K. BOWEN, *J. Mater. Sci.* **23** (1988) 2897.
33. H. U. ANDERSON, *J. Am. Ceram. Soc.* **50** (1967) 235.
34. E. A. BARRINGER, R. BROOK and H. K. BOWEN, in "Sintering and Heterogeneous Catalysis", edited by G. C. Kuczynski, A. E. Miller and G. A. Sargent (Plenum Press, New York, 1983) p. 1.
35. P. DURAN, P. RECIO, J. R. JURADO, C. PASCUAL and C. MOURE, *J. Am. Ceram. Soc.* **72** (1989) 2088.

Received 9 January
and accepted 18 March 1996